Improving Power Captured of Variable Speed Wind Turbine by using Adaptive Control Algorithm

Mebiratu Allo Begawo[1], Gete Tesfaye Zelie[2]

[1]*Master's Scholar in Control and Instrumentation engineering at Hawassa University, Institute of technology, Hawassa, Ethiopia*
[2]*M.Sc. in power system engineering at Assosa University College of Engineering, Assosa, Ethiopia*

Abstract: **Wind energy generated by using wind as a fuel is clean and non-polluting as a result it has become more widespread today. However, the uncertainty in the aerodynamic parameters makes the wind energy to cost more. Many researches have been done to increase the wind turbine efficiency, but they fail to consider this uncertain aerodynamic parameters. In this paper an adaptive control technique, which resembles the existing quadratic controller used by the wind industry for variable speed wind turbines below rated power, is designed to reduce the negative effects of this uncertainty. This adaptive controller uses a simple, highly intuitive extremum seeking scheme designed to seek out the optimal gain for maximizing the turbine's energy capture. The adaptive controller has been tested and validated using MATLAB simulation.**

Key terms: **adaptive control, extremum seeking scheme, gradient, stability, variable speed wind turbine**

I. INTRODUCTION

Wind energy is a rapidly growing renewable energy source within the world today. The process of wind power generation will never release any pollutants to the atmosphere, thus it does not yield any end-results, which could damage the environment. Nowadays, wind turbines must contend with various other energy generations. Hence, they should produce power with less cost. The wind turbine efficiency can be increased by developing advanced and sophisticated control algorithms. The focus of this report is the design of an adaptive controller to maximize energy capture at lower wind speeds. Wind turbines can be divided according to the orientation of the spin axis in to horizontal and vertical axis type turbines. Horizontal axis wind turbines (HAWT) are the most commonly used turbines today. They have an axis of rotation parallel with the wind stream. Whereas vertical axis wind turbines have an axis of rotation perpendicular to the wind direction and they are less commonly used [1]. Based on operating mode wind turbines can be classified as constant and variable speed wind turbines. In constant speed wind turbines the rotor turns at a specified constant speed. Because of the constrained rotor speed the optimum aerodynamic efficiency cannot be achieved at all wind speeds. On the other hand, variable-speed wind turbines run at optimal efficiency because rotor speed is made proportional to the wind speed (below its rated wind speed) [2]. There are three basic regions of operation in variable speed wind turbines as shown from figure 1.

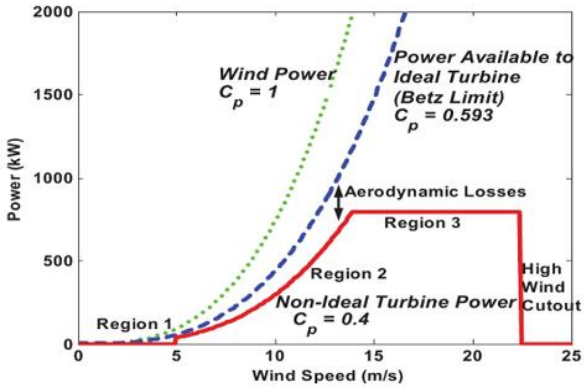

Figure 1: Steady state power curves [3]

Although, the principle of variable speed wind turbines are better than constant wind turbines, the uncertainty in the aerodynamic parameters can cause variable speed wind turbines to capture even less power than constant speed turbines at lower wind speeds if the controller used is not advanced. Therefore, the main objective of this research is to design an adaptive controller algorithm that can maximize the power capture of variable speed wind turbine in region 2 (i.e. at wind speeds lower than rated wind speed).

Many researchers have developed methods for limiting power and speed in region 3 such as speed regulation of wind turbines by Stol and Balas [4], Hand [6] and feedback linearization control for wind turbine by kumar and stol [8]. Okedu, K. E [5] and Karakasis, N., *et al* [7] proposed new schemes for Optimizing wind turbine performance. Although, they are effective in achieving their corresponding control objectives, they fail to consider the uncertain aerodynamic behavior of variable speed wind turbines which is common from real turbines. Quadratic controllers, such as those presented by Freeman and Balas [9], Song *et al.* [10] and pitch and torque control of variable speed wind turbine by Arkadiusz Kulka [11], force the turbine to track a desired rotor speed in region 2 by assuming that the values of C_{pmax} and the corresponding λ_* value is known. But the fact that those two parameters are not well known is a major source of energy loss in region 2 when these controllers are employed. Fuzzy predictive controller developed by Zhang *et al* [12] sufficiently maintains the rotor speed at its optimal value by minimizing the cost function. However the study have a drawback in that the optimal rotor speed is assumed to be

known priori when deigning the controller, but in fact it could change with turbine behavior.

The paper is organized as follows. In section two the mathematical modeling of aerodynamic part of variable speed wind turbine is developed and is validated by comparing its performance with the validated model of Sany wind turbine which is found from Adama II wind turbine generation system (WTGS). In section three the drawback of the existing quadratic controller is discussed, the proposed adaptive controller (i.e. Extremum seeking scheme) is designed and the stability analysis of the proposed adaptive controller is discussed. In section four the Simulink block diagram of the control algorithm and the discussion of the simulation results is presented. Finally, the conclusions are presented in the section five.

II. SYSTEM MODELING AND VALIDATION

The system block diagram shown from figure 2 consists of two main blocks, such as turbine model blocks (non-linear aerodynamic model and linear turbine model) and turbine controller block (extremum seeking scheme and generator torque control).

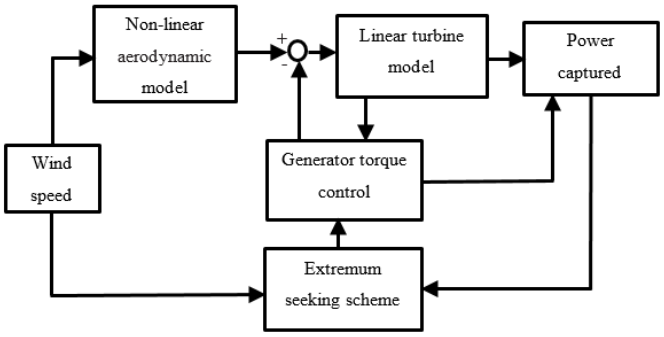

Figure 2: A block diagram model of the turbine and the proposed controller system

A. Mathematical Modeling of Wind Turbine

Figure 3 shows the wind energy conversion system used to drive the mathematical modeling of the variable speed wind turbine. In this research it is assumed that the generator output torque is accurately controlled so that it tracks its reference value. A relationship between the output power and the various variables constitute the mathematical model of the wind turbine.

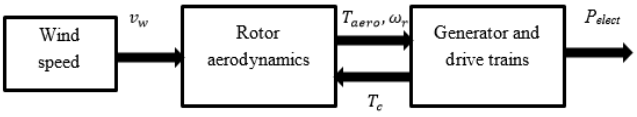

Figure 3: A typical wind energy conversion system [13]

The kinetic energy (KE) in air of an object of mass *m* moving with speed *v* is equal to:

$$KE = \frac{1}{2}mv^2 \quad (1)$$

The KE (in joules) of wind for the mass *m* and velocity v_w can be calculated by using (1). Therefore the power p_w in the wind can be given as:

$$p_w = \frac{dE}{dt} = \frac{1}{2}\frac{dm}{dt}v_w^2 \quad (2)$$

But mass flow rate is given by $\frac{dm}{dt} = \rho A v_w$ where *A* is the area through which the wind in this case is flowing and ρ is the density of air, then (2) becomes:

$$p_w = \frac{1}{2}\rho A v_w^3 \quad (3)$$

The actual mechanical power (p_{ext}) extracted by the rotor blades in watts is the difference between the upstream and the downstream wind powers [14], i.e.

$$p_{ext} = \frac{1}{2}\rho A v_w (v_u^2 - v_d^2) \quad (4)$$

Where, v_u is the upstream wind velocity at the entrance of the rotor blades in m/s and v_d is the downstream wind velocity at the exit of the rotor blades in m/s and v_w being the average of the velocities v_u and v_w. From the mass flow rate, we may write:

$$\rho A v_w = \frac{\rho A (v_u + v_d)}{2} \quad (5)$$

With this expression, (4) becomes $p_{ext} = \frac{1}{2}\frac{\rho A (v_u + v_d)}{2}(v_u^2 - v_d^2)$, which after a little simplification becomes:

$$p_{ext} = \frac{1}{2}\rho A v_w^3 C_p \quad (6)$$

Where, $C_p = \frac{1 - \left(\frac{v_d}{v_u}\right)^2 + \frac{v_d}{v_u} - \left(\frac{v_d}{v_u}\right)^3}{2}$

C_p is often called the Betz limit after the Germany physicist Albert Betz who worked it out in 1919. Other names for this quantity are the power coefficient of the rotor or rotor efficiency. The Betz limit says that no wind turbine can convert more than 59.3% of the kinetic energy of the wind into mechanical energy turning a rotor, i.e. $C_{pmax} = 0.59$. Wind turbines cannot operate at this maximum limit though. The power coefficient C_p is the most important parameter in the design of wind power plants. The model of C_p is [15]:

$$C_p(\lambda, \beta) = c_1\left(c_2\frac{1}{\gamma} - c_3\beta - c_4\beta^x - c_5\right)e^{-c_6\frac{1}{\gamma}} \quad (7)$$

Where, the values of the coefficients $C_1 - C_6$ depend on turbine type. In this thesis, the following values have been used, $C_1 = 0.5$, $C_2 = 90.1$, $C_3 = 0.4$, $C_4 = 0$, $C_5 = 5$, $C_6 = 15$

γ is defined by [15]:

$$\frac{1}{\gamma} = \frac{1}{\lambda + 0.08*\beta} - \frac{0.035}{1 + \beta^3} \quad (8)$$

The aerodynamic torque can be found as:

$$T_{aero} = \frac{1}{2}\rho A R^3 (C_p(\lambda, \beta)/\lambda^3)\omega^2 \quad (9)$$

This aerodynamic torque is divided into torque of rotor inertia and generator (control) torque i.e. $T_{aero} = J\dot{\omega} + Tc$.

Considering a simple rigid body model of a wind turbine and rearranging the above expression we can obtain the dynamic equation relating net torque and angular acceleration as:

$$\dot{\omega} = 1/J(T_{aero} - Tc) \quad (10)$$

Substitute (11) into (12) to obtain the following dynamic equation:

$$\dot{\omega} = 1/J(\tfrac{1}{2}\rho AR^3(C_p/\lambda^3)\omega^2 - Tc) \quad (11)$$

The diagram of the wind turbine model designed by using MATLAB's software, Simulink, as shown in the figure 4

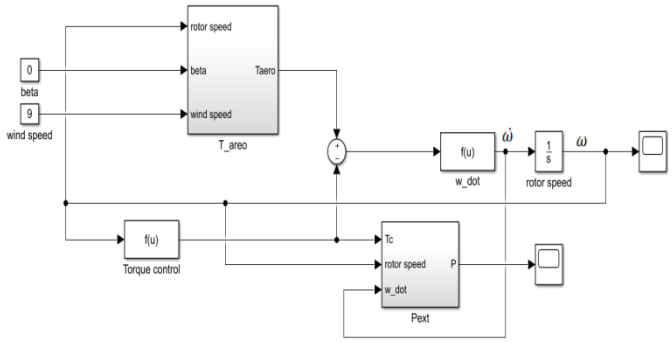

Figure 4: Block diagram of wind turbine model by using Simulink

B. Model Validation

There are two ways to validate the developed models: either by comparing the model's output to the output of an already validated model, or by comparing the model's output to real turbine data. In this paper the output of the validated model of Sany wind turbine, which is found from Adama II wind turbine generation system (WTGS), is used to compare the output of the developed model and then to validate it.

Figure 5 shows the plot of the output power of the developed model and the Snay wind turbine. As it is seen from the figure the two curves are similar and the visible small difference is expected because of the following reasons: the power coefficient modeling error, the unconsidered yaw error and the variation in efficiency of hub, speedup gearbox and generator. Except the yaw error that can be compensated by yaw control, which is not a part of the thesis, the error due to the remaining two reasons will not affect the proposed control algorithm. Because, the entire motivation behind the proposed adaptive controller is that the turbine's power coefficient is not well determined and failure to have an accurate model is the result of these uncertainties. Therefore, in spite of the above error we can still take the model as a valid model to test the proposed control algorithm.

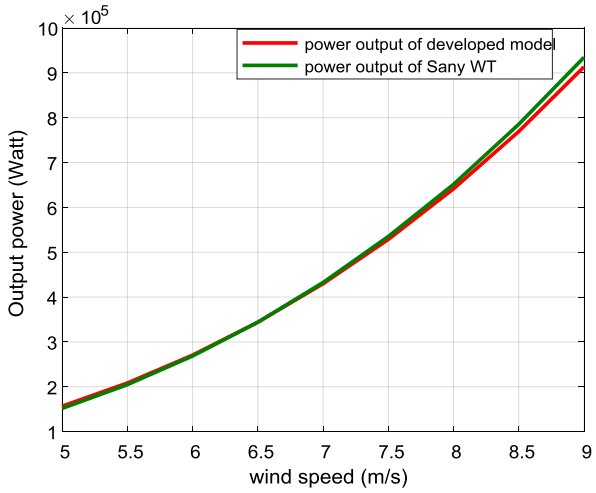

Figure 5: power output of sany WT and the developed model

III. CONTROLLER DESIGN AND STABILITY ANALYSIS

A. Controller Design

Before going to the design part of the proposed controller first let us see about the nature and drawback of the existing quadratic controller. A control law, which we refer to as the quadratic control, is to let the control torque T_c (that is, the generator torque) be given by $T_c = k_c\omega^2$, where, the expression of k_c is given by $k_c = \frac{1}{2}\rho AR^3\frac{C_{pmax}}{\lambda_*^3}$. Substitute this control law into (13) and rearrange to obtain $\dot{\omega} = \frac{1}{2J}\rho AR^3\omega^2(\frac{C_p}{\lambda^3} - \frac{C_{pmax}}{\lambda_*^3})$. From this equation J, ρ, A, R, and ω^2 are all nonnegative, hence the sign of $\dot{\omega}$ depends on the sign of the difference within the parentheses. It is fact that $C_p \le C_{pmax}$. Thus, when $\lambda \ge \lambda_*$ $\dot{\omega}$ will be negative and the rotor will decelerate towards $\lambda = \lambda_*$. On the other hand, if $\lambda < \lambda_*$ $\dot{\omega}$ will be positive and the rotor will accelerate towards $\lambda = \lambda_*$ when $C_p \ge \frac{C_{pmax}}{\lambda_*^3}\lambda^3$.

The existing quadratic controllers force the turbine to track a desired rotor speed in region 2 by assuming that the values of C_{pmax} and the corresponding λ^* value is known (i.e. the value the gain k_c is constant). However, the fact that those two parameters are not well known is a major source of energy loss in region 2 when these controllers are employed.

The main quality of the extremum seeking controller which is going to be designed in this thesis is that it attempts to have the turbine power track the wind power but assumes the values of C_{pmax} and the corresponding λ value is unknown (i.e. the value of k_c is varying with respect to the power coefficient curve). By this manner the problem of energy loss in region 2 can be addressed. The expression of the torque control law is similar with that of the quadratic controller as shown in (14), where the gain k_c is replaced by the letter G.

$$Tc = \begin{cases} 0 & \omega < 0 \\ G\omega^2 & \omega \ge 0 \end{cases} \quad (14)$$

Where, the adaptive gain G has the same expression as that of the control gain k_c.

In this paper a new concept of fraction of power captured (C_{pf}) is used to calculate the fraction of electrical power captured from the wind turbine. It is computed as electrical power produced per wind power, i.e.

$$C_{pf} = \frac{p_{elect}}{p_w} \quad (15)$$

Where, p_{elect} = over all turbine efficiency $(\eta) * p_{ext}$, and η is computed as: $\eta = \eta_h * \eta_{gb} * \eta_g$, Where, η_h, η_{gb} and η_g represents the hub efficiency, the gearbox efficiency and the generator efficiency respectively. Their corresponding values in percent, which are found from the nameplate data of Sany wind turbine located from Adama II WTGS, are 96, 97, 97 respectively. Then the value of η can be determined as:

$$\eta = (0.96 * 0.97 * 0.97) * 100\ \% \approx 90\%$$

This value of η can be interpreted as, about 90% of mechanical power extracted by the wind turbine is converted into electrical power. However, this efficiency value is not fixed, such that it may vary over time with respect to wind turbine's age. But the proposed adaptive control algorithm is able to respond to this kind of wind turbine behavior change by adapting the gain to new optimal operating point. In other words, this value of η is considered as the initial efficiency value to start the simulation.

A simulation is conducted by using the dynamic equation of wind turbine from (11) and a torque control law equation from (14) under different gain (G) values for a developed model of Sany WT which can generate a maximum power of 1.5MW at rated wind speed of 12m/s. The result is plotted as fraction of power produced versus normalized gain G ($\frac{G}{\bar{G}}$) for each of different gain values as shown in figure 6. Where, $\bar{G}$ is the assumed optimal operating point based on the standard control law coefficient k.

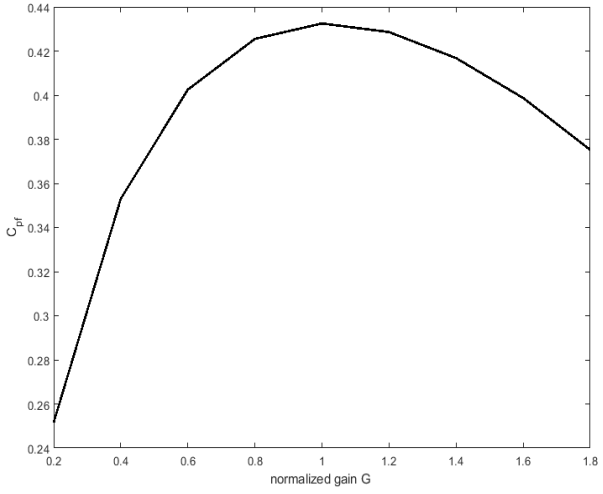

Figure 6: C_{pf} Vs normalized gain G ($\frac{G}{\bar{G}}$) graph

As it is seen from the graph of C_{pf} Vs normalized gain, initially the fraction of power produced increases until the optimal value of G is reached and after which it starts to decrease. The performance characteristic 'fraction of power produced (C_{pf})' and power coefficient C_p are closely related. Therefore, it is possible to conclude that C_{pf} will be maximum when the extracted power from the wind is maximum. Hence, C_{pf} is critically important variable in the analysis done in this thesis.

Extremum Seeking scheme is capable of dealing with unknown plants whose input to output maps possess an extremum (a minimum or a maximum), and this extremum depends on some parameter. Since the graph shown in Figure 6 possess a maximum point and the objective is to make the wind turbine to operate at this maximum value of C_{pf} we can use extremum seeking or self-optimizing scheme with sinusoidal perturbation to achieve the objective the paper.

1) An intuitive explanation about Extremum Seeking Scheme: Suppose we have an unknown map $f(\theta_p)$. All we know about this map is that it has a maximum, but the value of this maximum and $\theta_p = \theta_p^*$ at which it occurs are both unknown to us. We would like to find the value of θ_p^* that maximizes this map. The output of the map from Figure 7 is fed to a washout filter. The purpose of this filter is to remove the bias of the map from the origin. The signal is then demodulated and modulated by a sinusoidal perturbation and integrated to estimate θ_p^* and the result is fed back to $f(\theta_p)$. $f(\theta_p)$ is also referred to as the cost function. Running this loop several times will lead to the exponential convergence of θ_p to θ_p^*.

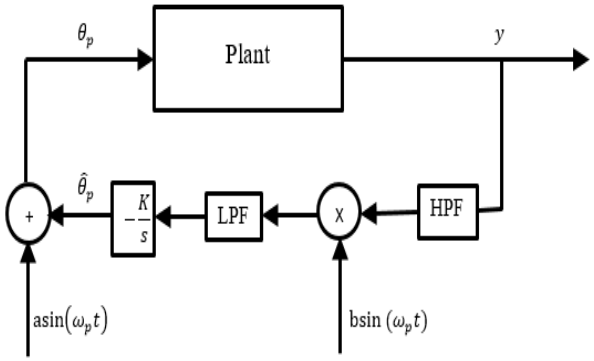

Figure 7: Basic extremum seeking loop [16]

2) Design of Extremum Seeking Scheme: The method of sinusoidal perturbation is the only method that permits fast convergence to the extremum on a time-scale comparable to that of the plant dynamics, which is a major advantage over the numerically based methods that require the plant dynamics to settle down prior to optimization [17, 18].

The idea is to add a small signal (sometimes called perturbation signal) to the gain (parameter to be estimated ($\hat{G}$)) and then measure the change in the output (C_{pf}) with respect to this signal. Based on this change, it will be decided whether to increase or decrease the gain (estimated parameter ($\hat{G}$)). Many methods adopt this approach, of which the gradient-based method is the most famous one and is used in this paper.

In the gradient-based approach, the gradient of the output with respect to the gain G (i.e.,$\frac{\partial C_{pf}}{\partial G}$) is estimated and used to determine the direction of change in the estimated gain $\hat{G}$. The gradient of the output with respect to the gain G ($\frac{\partial C_{pf}}{\partial G}$) is positive for values below the optimum, negative for values above the optimum and zero at the optimum point. The objective is making the plant to operate at the optimum point.

The plant model can be rewritten as follows.

$$\dot{\omega} = f(\omega, Tc) \tag{16}$$

$$Tc = \alpha(\omega, G) \tag{17}$$

$$C_{pf} = h(\omega) \tag{18}$$

Where, (18) is the unknown objective (performance index) function which is going to be maximized online.

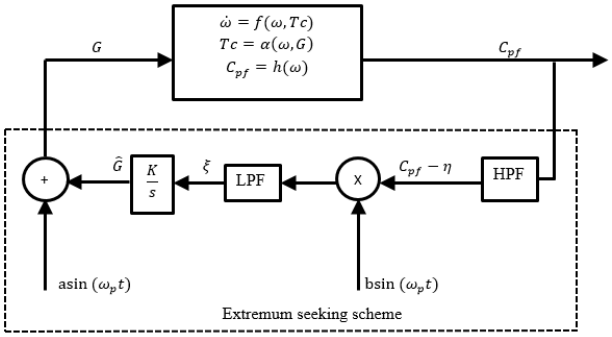

Figure 8: Gradient based ES scheme using BPF to find the gradient

As shown in figure 8, a high pass filter (HPF), a multiplier, and a low pass filter (LPF) are used to estimate $\frac{\partial C_{pf}}{\partial G}$. To understand the operation of the approach let us assume the perturbation signal amplitude a is very small and that the estimated gain $\hat{G}$ is almost constant with respect to the perturbation signal. Indeed large values for a and K allow faster convergence rates, but respectively increase the oscillation amplitude and sensitivity to disturbances. The plant output (C_{pf}) can be approximated by a first-order Taylor series near the estimated parameter $\hat{G}$ as:

$$C_{pf} = C_{pfo} + \frac{\partial C_{pf}}{\partial G}(G - \hat{G}) \tag{19}$$

But to obtain the plant input (estimated gain) G a slow perturbation signal $a\sin(\omega_p t)$ is added to the signal $\hat{G}$, which is the current best estimate of the optimum gain G^*, as given in (20).

The perturbation signal should be slow enough so that the plant appears as a static map to the cost function and the dynamics do not interfere to the peak seeking scheme. Therefore, the plant dynamics in (16) appear as instantaneous and the objective function in (18) reduces to $C_{pf}(G)$. Subsequently, the perturbation amplitude is selected so as to obtain small steady state output error.

$$G = \hat{G} + a\sin(\omega_p t) \tag{20}$$

Where, ω_p is the perturbation frequency.

After substituting (20) into (19) the plant output equation can be rewritten as:

$$C_{pf} = C_{pfo} + a\frac{\partial C_{pf}}{\partial G}\sin(\omega_p t) \tag{21}$$

The filter cut-off frequencies must be designed in coordination with the perturbation frequency ω_p. The purpose of HPF is to attenuate the DC component of the cost function while preserving the perturbation frequency (ω_p) should be in the pass band of the filter. Therefore, its cut-off frequency should be selected as $\omega_h < \omega_p$, where ω_h is the cut-off frequency of HPF. Then HPF is expressed as $\frac{s}{s+\omega_h}$. The expression of the output (cost) function after HPF is depicted in (22).

$$C_{pf} = a\frac{\partial C_{pf}}{\partial G}\sin(\omega_p t) \tag{22}$$

After multiplying (22) by a modulation signal $b\sin(\omega_p t)$ the following expression will be obtained:

$$C_{pf} * b\sin(\omega_p t) = a\frac{\partial C_{pf}}{\partial G}\sin(\omega_p t) * b\sin(\omega_p t) = \frac{ab}{2}\frac{\partial C_{pf}}{\partial G} - \frac{ab}{2}\frac{\partial C_{pf}}{\partial G}\cos(2\omega_p t) \tag{23}$$

By selecting an appropriate cut-off frequency of LPF to filter out $\cos(2\omega_p t)$ its output can be approximated by $\frac{ab}{2}\frac{\partial C_{pf}}{\partial G}$ which is proportional to the gradient $\frac{\partial C_{pf}}{\partial G}$. If ω_l is selected as the cut of frequency of the LPF, the expression of LPF is given as $\frac{\omega_l}{s+\omega_l}$. Now given an estimate of the gradient $\frac{\partial C_{pf}}{\partial G}$ (i.e. ξ), it is required to control G in such a way that drives $\frac{\partial C_{pf}}{\partial G}$ to zero. Therefore, the signal ξ can be thought of as the sensitivity $\frac{ab}{2}\frac{\partial C_{pf}(\hat{G})}{\partial G}$ and the gradient update law used to force $\hat{G}$ to G^* is: $\dot{\hat{G}} = k\frac{ab}{2}\frac{\partial C_{pf}(\hat{G})}{\partial G}$. The selection criteria for the parameters $a, b, \omega_p, \omega_h, \omega_l$ and k is illustrated in more detail in section 3.2.

B. Stability Analysis

By substituting (17) into (16) and by using the expression of G from (20), we will have the following expression:

$$\dot{\omega} = f(\omega, \alpha(\omega, \hat{G} + \text{asin}(\omega_p t))) \quad (24)$$

Now let us make some assumptions about the existence and stability of an equilibrium point similar to those made in [19].

Assumption 1: There exists a smooth function $l: \mathbb{R} \to \mathbb{R}$ such that

$f\left(\omega, \alpha\left(\omega, \hat{G} + \text{asin}(\omega_p t)\right)\right) = 0$ If and only if $\omega = l(G)$.

Assumption 2: For each $G \in \mathbb{R}$, the equilibrium $\omega = l(G)$ of the system is locally exponentially stable.

The function composition $C_{pf} = (hol)(G) = h(l(G))$ represents the steady state static map of the system, which leads to the third assumption.

Assumption 3: There exists $G^* \in \mathbb{R}$ such that

$$\frac{\partial}{\partial G}(hol)(G^*) = 0$$
$$\frac{\partial^2}{\partial G^2}(hol)(G^*) < 0$$

Assumption 3 is the condition required for the static map $C_{pf} = (hol)(G)$ to have a maximum at G^*.

If we use a slow perturbation signal $\text{asin}(\omega_p t)$, then the plant appears as static map $C_{pf} = (hol)(G)$ as shown in Figure 9 and its dynamics do not interfere with the peak seeking scheme.

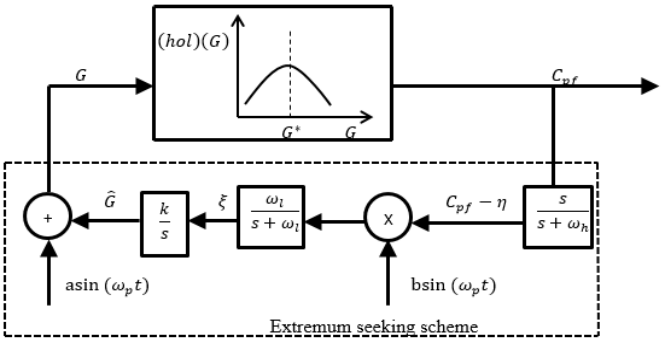

Figure 9: A plant as static map when the perturbation is slow

We can now combine and rewrite the equations of the system with the equations of the proposed controller as given below:

$$\frac{d\omega}{dt} = f(\omega, \alpha(\omega, \hat{G} + \text{asin}(\omega_p t))) \quad (25a)$$

$$\frac{d\hat{G}}{dt} = k\xi \quad (25b)$$

$$\frac{d\xi}{dt} = -\omega_l \xi + \omega_l (C_{pf} - \eta)\text{bsin}(\omega_p t) \quad (25c)$$

$$\frac{d\eta}{dt} = -\omega_h \eta + \omega_h C_{pf} \quad (25d)$$

Where, $(k, a, b, \omega_p, \omega_l, \omega_h)$ are tuning parameters. To simplify the theoretical analysis let assume that a and b are equal, but practically they may have different values, then the parametric space will be $(k, a^2, \omega_p, \omega_l, \omega_h)$.

The parameters of the controller will be selected as [19]

$$\omega_h = \omega_p \omega_H = \omega_p \delta \omega_H' = O(\omega_p \delta) \quad (26a)$$

$$\omega_l = \omega_p \omega_L = \omega_p \delta \omega_L' = O(\omega_p \delta) \quad (26b)$$

$$k = \omega_p K = \omega_p \delta K' = O(\omega_p \delta) \quad (26c)$$

Where ω_p and δ are small positive constants and ω_H', ω_L' and K' are $O(1)$ positive constants.

Now let us introduce the new coordinates that shifts the equilibrium or the optimal operating point to the origin:

$$\tilde{G} = \hat{G} - G^* \Rightarrow \frac{d\tilde{G}}{dt} = \frac{d\hat{G}}{dt} \quad (27)$$

$$\tilde{\eta} = \eta - hol(G^*) \Rightarrow \frac{d\tilde{\eta}}{dt} = \frac{d\eta}{dt} \quad (28)$$

By using (26) and (27) and time scale, $\tau = \omega_p t$ the system from (25) can be rewritten as:

$$\omega_p \frac{d\omega}{d\tau} = f(\omega, \alpha(\omega, \tilde{G} + G^* + \text{asin}(\tau))) \quad (29a)$$

$$\frac{d}{d\tau}\begin{bmatrix}\tilde{G}\\ \xi\\ \tilde{\eta}\end{bmatrix} = \delta\begin{bmatrix}K'\xi\\ -\omega_L'\xi + \omega_L'(h(\omega) - hol(G^*) - \tilde{\eta})\text{asin}(\tau)\\ -\omega_H'\tilde{\eta} + \omega_H'(h(\omega) - hol(G^*))\end{bmatrix} \quad (29b)$$

Where (a^2, δ, ω_p) are tuning parameters.

To show the stability of the above system in (29a) and (29b) steps similar to that of [19] are used. First the overall system is divided in to two time scales, the fast dynamics as in (29a) and the slow dynamics as in (29b). The fast dynamics will be frozen around the equilibrium point and its state variable is treated as constant in the slow dynamics. Since the slow dynamics have periodic behavior an averaging technique, which is the standard approach for analyzing periodic systems, is used to investigate its stability properties.

Freeze ω from (29a) to its equilibrium value, such that

$$\omega = l(G^* + \tilde{G} + \text{asin}(\tau)) \quad (30)$$

Substitute (30) into (29b) to obtain the following reduced system:

$$\frac{d}{d\tau}\begin{bmatrix}\tilde{G}_r\\ \xi_r\\ \tilde{\eta}_r\end{bmatrix} = \delta\begin{bmatrix}K'\xi\\ -\omega_L'\xi_r + \omega_L'(v(\tilde{G}_r + \text{asin}(\tau)) - \tilde{\eta})\text{asin}(\tau)\\ -\omega_H'\tilde{\eta} + \omega_H'(v(\tilde{G}_r + \text{asin}(\tau))\end{bmatrix} \quad (31)$$

Where, $v(\tilde{G}_r + \text{asin}\,\tau) = hol(G^* + \tilde{G} + \text{asin}\,\tau) - hol(G^*)$

In view of assumption 3 the following expressions about $v(\tilde{G}_r + \sin\tau)$ are true:

$$v(0) = hol(G^* + 0) - hol(G^*) = 0 \quad (32a)$$

$$v'(0) = (hol)'(G^*) = 0 \quad (32b)$$

$$v''(0) = (hol)''(G^*) < 0 \quad (32c)$$

System in (31) is in the form to which averaging method is applicable. According to average model definition (from equation (10.25) of [20]), we can have the following average model of our system from (29):

$$\frac{d}{d\tau}\begin{bmatrix}\tilde{G}_r^a \\ \xi_r^a \\ \tilde{\eta}_r^a\end{bmatrix} = \delta\begin{bmatrix}K'\xi_r^a \\ -\omega_L'\xi_r^a + \frac{\omega_L'}{2\pi}a\int_0^{2\pi}(v(\tilde{G}_r^a + \sin\alpha))\sin\alpha d\alpha \\ -\omega_H'\tilde{\eta}_r^a + \frac{\omega_H'}{2\pi}\int_0^{2\pi}(v(\tilde{G}_r^a + \sin\alpha))d\alpha\end{bmatrix} \quad (33)$$

First let us determine the equilibrium point $(\tilde{G}_r^{a,e}, \xi_r^{a,e}, \tilde{\eta}_r^{a,e})$ of the average model in (33) which satisfies:

$$\xi_r^{a,e} = 0 \quad (34a)$$

$$\int_0^{2\pi}(v(\tilde{G}_r^{a,e} + \sin\alpha))\sin\alpha d\alpha = 0 \quad (34b)$$

$$\tilde{\eta}_r^{a,e} = \frac{1}{2\pi}\int_0^{2\pi}\left(v\left(\tilde{G}_r^{a,e} + \sin\alpha\right)\right)d\alpha \quad (34c)$$

Let us postulate $\tilde{G}_r^{a,e}$ in the following form [19]

$$\tilde{G}_r^{a,e} = b_1 a + b_2 a^2 + O(a^3) \quad (35)$$

After applying Taylor series expansion, integrating and equating like powers of a we will obtain $b_1 = 0$ and $b_2 = -\frac{v'''(0)}{8v''(0)}$, which implies that:

$$\tilde{G}_r^{a,e} = -\frac{v'''(0)}{8v''(0)}a^2 + O(a^3) \quad (36)$$

Following similar procedures for $\tilde{\eta}_r^{a,e}$ we will obtain $b_1 = 0$ and $b_2 = \frac{v''(0)}{4}$, which implies that:

$$\tilde{\eta}_r^{a,e} = \frac{v''(0)}{4}a^2 + O(a^3) \quad (37)$$

Then the required equilibrium point of the average model will be:

$$\begin{bmatrix}\tilde{G}_r^{a,e} \\ \xi_r^{a,e} \\ \tilde{\eta}_r^{a,e}\end{bmatrix} = \begin{bmatrix}-\frac{v'''(0)}{8v''(0)}a^2 + O(a^3) \\ 0 \\ \frac{v''(0)}{4}a^2 + O(a^3)\end{bmatrix} \quad (38)$$

The Jacobian of (33) at the equilibrium point $(\tilde{G}_r^{a,e}, \xi_r^{a,e}, \tilde{\eta}_r^{a,e})$ is:

$$J_r^{a,e} = \delta\begin{bmatrix}0 & K' & 0 \\ \frac{\omega_L'}{2\pi}a\int_0^{2\pi}(v'(\tilde{G}_r^{a,e} + \sin\alpha))\sin\alpha d\alpha & -\omega_L' & 0 \\ \frac{\omega_H'}{2\pi}\int_0^{2\pi}\left(v'\left(\tilde{G}_r^{a,e} + \sin\alpha\right)\right)d\alpha & 0 & -\omega_H'\end{bmatrix} \quad (39)$$

After a little simplification we will obtain the following characteristic polynomial of $J_r^{a,e}$:

$$char(J_r^{a,e}) = (\lambda_a + \delta\omega_H')(\lambda_a{}^2 + \lambda_a\delta\omega_L' - \delta^2K'\frac{\omega_L'}{2}a^2v''(0) + O(\delta^2a^3)) \quad (40)$$

Since we know from (32c) that $v''(0) < 0$, $J_r^{a,e}$ is Hurwitz for sufficiently small a (i.e. all roots of the characteristic polynomial of $J_r^{a,e}$ have negative real parts) which indicates that the equilibrium of average model is exponentially stable for sufficiently small a. Then, according to averaging theorem (Theorem 8.3 of [20]) we have that the solutions of the original system (i.e. $\tilde{G}_r, \xi_r, \tilde{\eta}_r$) and in particular their $\tilde{G}_r$ components, from (31), converges to an $O(\delta + a^2)$ neighborhood of the origin.

From this stability analysis a convergence error of $\tilde{G}_r^{a,e} = -\frac{v'''(0)}{8v''(0)}a^2 + O(a^3)$ is obtained. But these presents a drawback when a large perturbation signal is used. In [21] the modulation signal $g(\omega_p t)$ other than the traditional $sin(\omega_p t)$ is suggested to eliminate or reduce the convergence error without affecting the above stability condition. Note that the modified $g(\omega_p t)$ replaces the modulation signal while the perturbation signal is still $asin(\omega_p t)$. The modulation signal is modified as in the following proposition.

Under Assumption 3, the integration $\int_0^{2\pi}(v(\tilde{G}_r^{a,e} + \sin\alpha))gad\alpha$ is equal to zero at $Gra,e=0$ if the modulation signal $g(\alpha)$ is chosen as a sum of sinusoids.

$$g(\alpha) = \sum_{m=0}^{\overline{m}}(2m+1)sin((2m+1)\alpha) \quad (53)$$

Where, $m = 0, 1, 2, \ldots, \overline{m}$ And $\alpha = \omega_p t$

$\overline{m}$ is selected small enough so that the dynamics of the controller will not interfere to the plant dynamics (i.e. the dynamics of the plant is fast compared with the controller).

IV. RESULTS AND DISCUSSION

The simulation is compiled for the Sany wind turbine (SE7715) which can extract a maximum electrical power of 1.5MW at rated wind speed of 12m/s. The first three terms of $g(\omega_p t)$ is taken as a modulation signal (i.e. $\overline{m} = 3$). The remaining simulation parameters and their sample values are given in Table I.

Figure 10 and Figure 11 shows the simulation result of the rotor speed and the extracted power at 7m/s wind speed for both quadratic and adaptive (extremum seeking) controllers respectively. From Figure 10 and Figure 11 it is observed that

both controllers works similar at a theoretical or normal condition. However, small rise time and higher overshoot from the rotor speed and power extracted plot may happen due to the initial condition from the rotor speed plot in the case of the the extremum seeking controller. They make the rotor speed to increase from the initial value of 0.8rad/sec to 1.148rad/sec and results 477.5KW mechanical power to be extracted at wind speed of 7m/s. This result shows that the quadratic controller can give a desired result as that of the extremum seeking controller if C_{pmax} and λ^* are accurately known, but this is practically impossible because of the presence of aerodynamic uncertainties in the real turbine. Note that the choice of the value for the constant k depends on wind speed as well as on filter frequencies.

The wind turbine behavior change can be represented by its power coefficient change. For instance, if the C_{pmax} is changed from its optimal value of 0.4806 to 0.3845 for the Sany wind turbine as a result of turbine behavior change, the simulation results of rotor speed and the corresponding power extracted by extremum seeking and quadratic controllers will be as shown in Figure 12 and 13 respectively. As it is observed from Figure 12 and 13, when a change in the turbine behavior occurs the rotor speed of the turbine decreases from 1.148rad/s to 1.06rad/s and stays constant in the case of quadratic controllers. Whereas in the case of extremum seeking controller, the rotor speed is rising to retain its original speed value immediately after the change in the turbine's behavior is detected. Similarly, the power captured by the turbine changes from 477.5KW to 375.6KW if quadratic controller is used and it is changed from 477.5KW to 382KW if extremum seeking controller is used. This result shows that there is a power loss of 6.4kw if quadratic controller is used than extremum seeking controller.

Now let us see how the extremum seeking controller performs the gain adaptation law at normal condition as well as at the occurrence the turbine behavior change. The curves of the normalized adaptive gain (i.e. $\frac{G}{G^*}$) at a normal condition and during the turbine behavior change at wind speed of 7m/s are shown in Figure 14.

As it is shown from Figure 14 (a), at the normal condition the adaptive gain starts from its specified initial value (zero in this case) and is converging to its optimal value. However, Figure 14 (b) shows that when a change in the turbine behavior occurs the extremum seeking controller makes its gain G to adapt towards its new optimal value online while the system is operating, by which means it maximizes the power captured by the wind turbine.

The change in the weather condition may result for wind speed change due to wind gusts. The wind speed profile and the rotor speed of the turbine for both the existing quadratic and the proposed controllers, when a particular type of wind speed changes occurred due to wind gusts, are shown from Figure 15 and Figure 16 respectively.

As it is indicated from Figure 16 both controllers are capable of adjusting the rotational speed according to the wind speed variation to maintain the turbine's optimal operating point. This shows the robustness of the proposed controller for weather condition change.

Table I: Simulation Parameters

Description	Value
Cut-in wind speed	3.5m/s
Cut-out wind speed	25m/s
Rotor diameter	77.6m
Rated rotation speed	1.99rad/s
Rotor inertia (J)	$2.5 * 10\text{^}6\ kg.m^2$
Air density (ρ)	$1.225\ kg/m^3$
Optimal adaptation gain ($\bar{G}$)	315654.94
Initial rotor speed (ω_{init})	$0.8 rad/sec$
Perturbation amplitude (a)	0.01
Perturbation frequency (ω_p)	$1 rad/sec$
Integration gain (K)	0.79
HPF cut-off frequency (ω_h)	$0.6 rad/sec$
LPF cut-off frequency (ω_l)	$0.8 rad/sec$

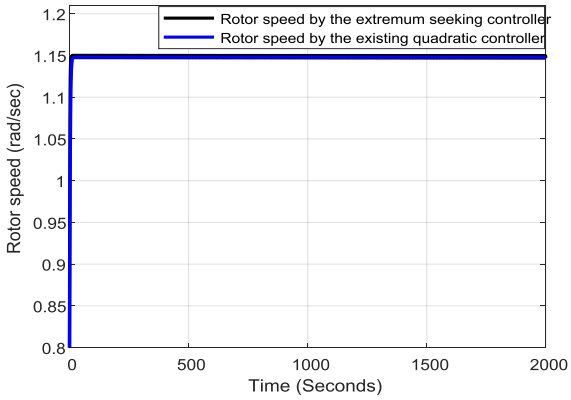

Figure 10: Rotor speed by the extremum seeking (black) and quadratic (blue) controllers

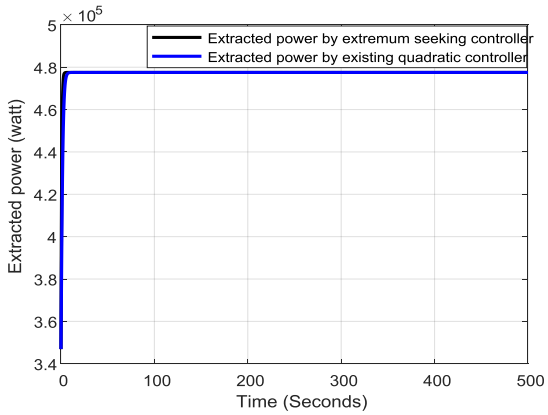

Figure 11: Power extracted by extremum seeking (black) and quadratic (blue) controllers

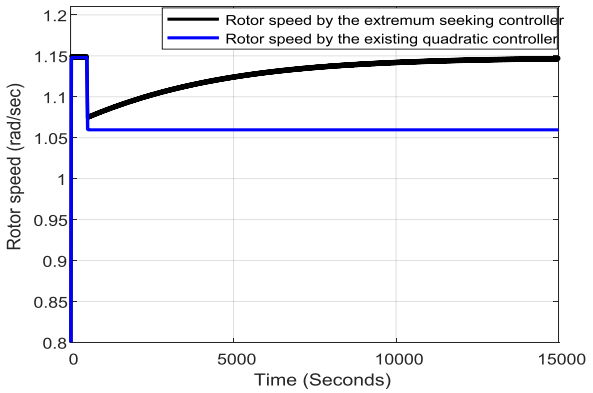

Figure 12: Rotor speed by extremum seeking (black) and quadratic (blue) controllers during turbine behavior change at 7m/s wind speed

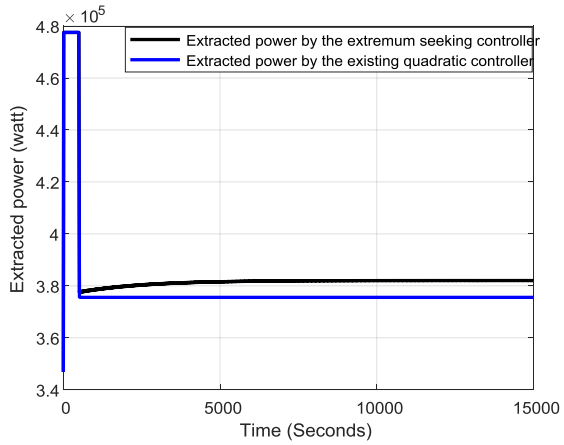

Figure 13: power extracted by extremum seeking (black) and quadratic (blue) controllers during turbine behavior change at 7m/s wind speed

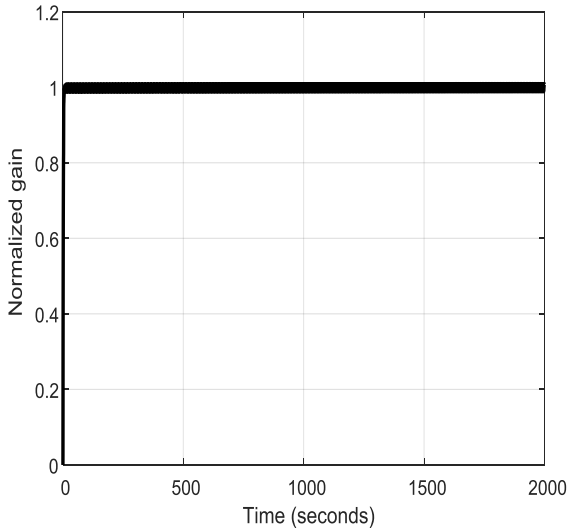

(a) Normalized adaptive gain at a normal condition

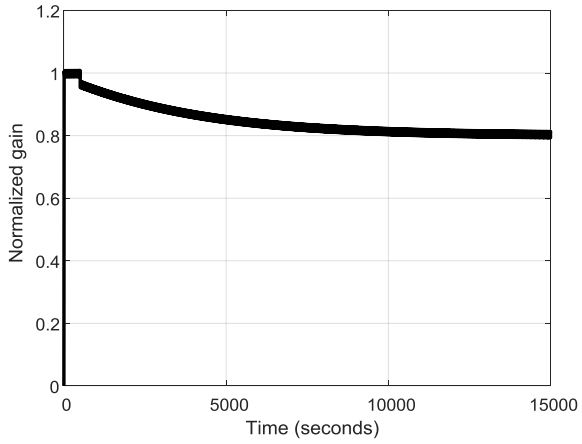

(b) Normalized adaptive gain during turbine behavior change

Figure 14: Normalized adaptive gain

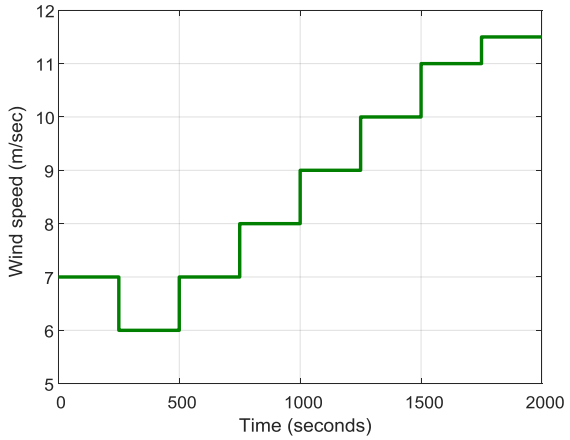

Figure 15: Wind speed profile for a change in weather condition

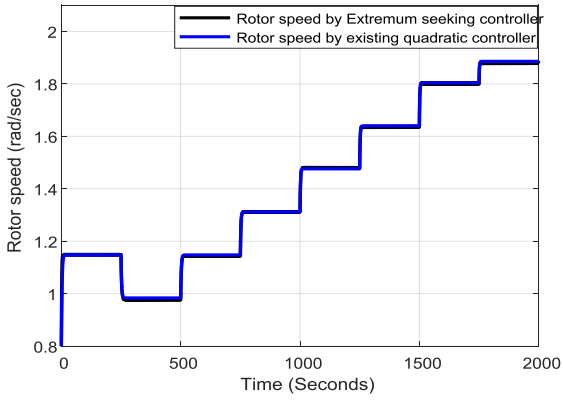

Figure 16: Rotor speed by the existing quadratic and extremum seeking controllers

V. CONCLUSION

In this paper an adaptive controller (extremum seeking controller) to optimize power captured of variable speed wind turbine is designed, analyzed and tested by simulation. It is

aimed to diminish energy loss in region 2 operation of the turbine due to the uncertainty of the aerodynamic parameters. As we observed from the simulation results the existing quadratic controller will function well only if the aerodynamic property of the wind turbine is fixed or not changing forever. However, this is unexpected practically because, the turbine's behavior is changing from time to time as result of bug build up and blade erosion and the inaccuracy present in the modeling of wind turbine. Because of this uncertainty sub-optimal energy capture will happen when the quadratic controllers are employed. However, we have seen that the Extremum seeking controller is able to reduce the problem due to the uncertain turbine behavior. Generally, the percentage improvements achieved by the Extremum seeking controller over the existing quadratic controller during the turbine behavior changes are 8.3% and 1.7% for the rotor speed and the extracted power respectively.

ACKNOWLEDGMENT

Primarily we would like to thank the almighty GOD for protecting us, granting us strength and courage to complete our study and in every step of my life.

REFERENCES

[1] An overview of wind energy status. Ackermann and Harrison, 2000

[2] Jenkins, N. Walker, J. (1997) *Wind Energy Technology*. Wiley, England.

[3] Wind turbine performance, control and design. AME 40530, University of Notre Dame.

[4] Stol, K., and Balas, M. 2002. "Periodic Disturbance Accommodating Control for Speed Regulation of Wind Turbines." Proceedings of the 21st ASME Wind Energy Symposium, Reno, NV, pp. 310-320.

[5] Okedu, K. E. (2020). Improving the transient performance of DFIG wind turbine using pitch angle controller low pass filter timing and network side connected damper circuitry", *IET Renew. Power Gener*. 14 (7), 1219–1227. doi:10.1049/iet-rpg.2019.1124

[6] Hand, M. 2003. Mitigation of Wind Turbine/Vortex Interaction Using Disturbance Accommodating Control. Ph.D. thesis, Boulder, CO: University of Colorado.

[7] Karakasis, N., *et al.*: ' Optimal efficiency control in a wind system with doubly fed induction generator', *IEEE Trans. Power Electron.*, 2019, 34, (1), pp. 356– 368

[8] A Kumar and K Stol. "simulating feedback linearization control of wind turbines using high-order models". *Wind Energy*, 13(5):419–432, 2010.

[9] Freeman, J., and Balas, M. 1999. "An Investigation of Variable Speed Horizontal-Axis Wind Turbines Using Direct Model-Reference Adaptive Control." Proceedings of the 18th ASME Wind Energy Symposium, Reno, NV, pp. 66-76.

[10] Song, Y., Dhinakaran, B., and Bao, X. 2000. "Variable Speed Control of Wind Turbines Using Nonlinear and Adaptive Algorithms." Journal of Wind Engineering and Industrial Aerodynamics, Vol. 85, pp. 293-308.

[11] Arkadiusz Kulka. " pitch and torque control of variable speed wind turbines". 2004

[12] Y. Zhang, Z. Yang and S. Haifei, "Fuzzy Predictive Control of Wind Turbine Systems Via Singular Perturbation Theory," in E3S Web of Conferences 72, 01008 (2018), Jinling Institute of Technology, 211169 Nanjing, China, 2018.

[13] Boukhezzar, B. Siguerdidjane, H. (2005) Nonlinear Control of Variable Speed Wind Turbines without wind speed measurement. *IEEE Conference on Decision and Control*

[14] Bossanyi, E. 1989. "Adaptive Control of the MS2 Wind Turbine. Practical Results." WindEngineering, Vol. 13, No. 5, pp. 259-273.

[15] Johnson, K., Fingersh, L., Balas, M., and Pao, L. 2004a. "Methods for Increasing Region 2Power Capture on a Variable Speed HAWT." Proceedings of the 23rd ASME Wind Energy Symposium, Reno, NV, pp. 103-113.

[16] Karrari, M. Malik, O. Rosehart, W. (2005) Comprehensive Control Strategy for a Variable Speed Cage Machine Wind Generation Unit. *IEEE Transactions on Energy Conversion* (Bajaro, 2011)

[17] K. Ariyur and M. Krstic, *Real-time optimization by extremum-seeking control*. WileyInterscience, 2003.

[18] W. Moase, C. Manzie, and M. Brear, "Newton-like extremum-seeking for the control of thermoacoustic instability," *Automatic Control, IEEE Transactions on*, vol. 55, no. 9, pp. 2094–2105, 2010

[19] M. Krstić and H. Wang, "Stability of extremum seeking feedback for general nonlinear dynamic systems," *Automatica*, vol. 36, no. 4, pp. 595–601, 2000.

[20] H. K. Khalil, *Nonlinear systems*. Prentice hall Upper Saddle River, 2002, vol. 3.

[21] Atta, khalid. "Extremum seeking control, stability, accuracy and applications", 2015